Physica A 410 (2014) 276–286

Contents lists available at ScienceDirect

Physica A

journal homepage: www.elsevier.com/locate/physa

On the dynamics of a tandem of asynchronous flapping wings: Lattice Boltzmann-immersed boundary simulations

Alessandro De Rosis *

Department of Agricultural Sciences (DIPSA), University of Bologna, 40127 Bologna, Italy

HIGHLIGHTS

- Numerical simulations are performed on a tandem of off-sync flapping wings.
- Scenarios accounting for the presence of a lateral wind gust are investigated.
- Increasing values of the wind gust tend to negatively affect the flight performance.
- For low values of the wind gust the tandem benefits from the asynchronous motion.

ARTICLE INFO

Article history:
Received 2 March 2014
Received in revised form 7 April 2014
Available online 20 May 2014

Keywords:
Fluid–structure interaction
Lattice Boltzmann method
Flapping wings
Immersed boundary

ABSTRACT

In this paper, the flight performance of a tandem of symmetric flapping wings immersed in a viscous fluid is investigated. A harmonic motion is imposed to the wings which can travel only in the vertical direction. Specifically, the attention focuses on the role of the initial phase difference. The fluid domain is modeled through the lattice Boltzmann method. In order to account for the presence of the wings immersed in the lattice fluid background, the immersed boundary method is adopted. Once fluid forces acting upon the wings are computed, their position is updated by solving the equation of solid motion by the time discontinuous Galerkin method according to a strategy already validated by the author. A wide numerical campaign is carried out by varying the initial phase difference. Moreover, scenarios accounting for the presence of a lateral wind gust are shown. The flight conditions and performance are discussed for a wide set of configurations and compared with an in-sync configuration, showing that the wind gust reduces the performance in certain scenarios.

1. Introduction

An effective computation of the lift generated in flapping wings by a prescribed motion is an attractive issue recently arosen in the computational fluid dynamics framework. In particular, this problem has practical applications in the design of micro-air vehicles and robotic drones which can be used in the mechanics, defense and even civil industry. Huge attention has been devoted to the role of the deformability of the wing. Specifically, Heathcote et al. [1,2] showed that a flapping wing benefits from flexibility, especially within a certain range of the Strouhal number. The impact of the flexibility on the aerodynamics performance was studied in Ref. [3], showing that aerodynamic forces can be controlled by altering the trailing edge flexibility of a flapping wing. More recently, Mountcastle et al. [4] and Kang et al. [5] underlined that the deformability plays a crucial role in the lift generation, enhancing the performance.

Among the possible aspects to be highlighted, one of the most intriguing is represented by the vorticity generated by the tip of the wing, which is responsible for a remarkable modification of the hydrodynamics surrounding the wing itself, thus

* Tel.: +39 3933069488.
E-mail address: alessandro.derosis@unibo.it.

http://dx.doi.org/10.1016/j.physa.2014.05.041
0378-4371/

leading to the generation of a useful support during the beat [6]. According to Ref. [7], the leading-edge vortexes represent a flow structure which is largely responsible for the performance of the wings. In Ref. [8,9] the particle image velocimetry technique has been applied to quantify the leading-edge vortexes in insects. The benefit induced by such vortexes has proved to be effective even for slow-flying bats [10]. The dynamic behavior of the tip-induced vortexes has been recently investigated in Ref. [11], showing how the vortex structure arises and develops during the wing beat. Trizila et al. [12] studied the aerodynamics of flapping wings by imposing a translation and a rotation to a rigid wing. Consequently, the induced vorticity and lift coefficient for different scenarios of the imposed motion have been analyzed, focusing on their relationship.

Concerning the flapping wing modeling, the lattice Boltzmann (LB) method [13] has been combined with the immersed boundary (IB) one [14] in a recent work [15], showing interesting results related to the interplay between two in-sync flapping wings. Moreover, the effect of a wind gust has been discussed, leading to the definition of a critical value inhibiting the take-off. The LB method is adopted to predict fluid dynamics, whereas the IB method is used to account for the presence of the wing in the lattice background. The IB method has been preferred to the well known interpolated bounce-back scheme [16,17], due to its superior properties in terms of stability and involved computational effort [18]. Specifically, for a given grid resolution the IB method has proved to be able to solve problems characterized by Reynolds numbers which are higher with respect to the ones achievable by using the bounce-back scheme. Moreover, the computation of the forces acting on a solid body is immediately available due to the intrinsic nature of the IB method, thus avoiding stress integration procedures which are known to involve high CPU time [18]. As discussed in Ref. [15,19], wing dynamics is computed via the time discontinuous Galerkin (TDG) method. This choice over standard Newmark or α schemes is motivated by higher stability, accuracy and convergence, as devised in Ref. [20]. The adopted numerical methods and the coupling strategy have been widely discussed and validated by the author for flow induced vibrations [21,22], blood flow [23], shallow waters [24] and even hull slamming [25]. The interested reader can refer to the above cited works for further details about the numerical methods.

In this work, the motion of a tandem of rigid flapping wings is numerically investigated by imposing a harmonic motion to the wings. Wings can travel only in the vertical direction. Specifically, the attention focuses on the difference in the initial phase angle, thus relating the flight performance to the asynchronous motion. Moreover, the effect of a constant uniform rightward wind gust is discussed, showing how the behavior is affected. A wide numerical campaign is carried out. In particular, the initial phase angle of one of the wings is kept fixed, while the other one varies. In addition, simulations characterized by increasing values of the wind gust are performed. Findings in terms of the time history of the position of the centers of mass are discussed, together with considerations about the velocity field.

Despite previous efforts [26–29], this work presents new insights. Specifically, the behavior of a tandem of butterfly-like wings is investigated, whereas the literature focuses mainly on isolated bodies. In this way, the mutual interaction between the wings is highlighted, together with the role of the encompassing hydrodynamics. Moreover, the effect of the asynchronous motion of a tandem of symmetric flapping wings is discussed here for the first time, showing that the flight performance of the butterfly-like body is considerably influenced by the initial phase angle of the other one, and vice versa. The paper is organized as follows. In Section 2, the problem is stated. In Section 3, the results of a numerical campaign are discussed. Finally, in Section 4 some conclusions are drawn.

2. Problem statement

A tandem of symmetric flapping wings is immersed in a fluid of viscosity ν and density ρ. According to Ref. [30,31], the following butterfly-like physical parameters corresponding to a *Pieris melete* are adopted:

- wing mass 3.5×10^{-6} kg;
- body mass 5.0×10^{-5} kg;
- hinge-wing distance 5.0×10^{-3} m;
- wing length $L = 3.0 \times 10^{-2}$ m.

Notice that the total mass is equal to $M = 5.7 \times 10^{-5}$ kg. Following the approach recently proposed by Ref. [15], the harmonic motion $\theta(t)$ defined as

$$\theta(t) = \Delta\theta \cos\left(\frac{2\pi t}{T} + \phi\frac{\pi}{180^\circ}\right), \tag{1}$$

is imposed to both the systems sketched in Fig. 1. Notice that $\Delta\theta = 46.8^\circ$ is the amplitude, $T = 0.1$ s is the period of the harmonic oscillation, ϕ is the initial phase angle and t is the time. Simulations are performed by setting $\phi = 0^\circ$ for A, whereas the initial phase angle of B varies.

2.1. Governing equations

The problem is governed by the Navier–Stokes equation for an incompressible flow. Specifically, such equations read as follows:

$$\nabla \cdot \mathbf{u} = 0, \tag{2}$$

$$\frac{\partial \mathbf{u}}{\partial t} + (\mathbf{u} \cdot \nabla)(\mathbf{u}) = -\frac{1}{\rho}\nabla(p) + \nu\nabla^2\mathbf{u}, \tag{3}$$

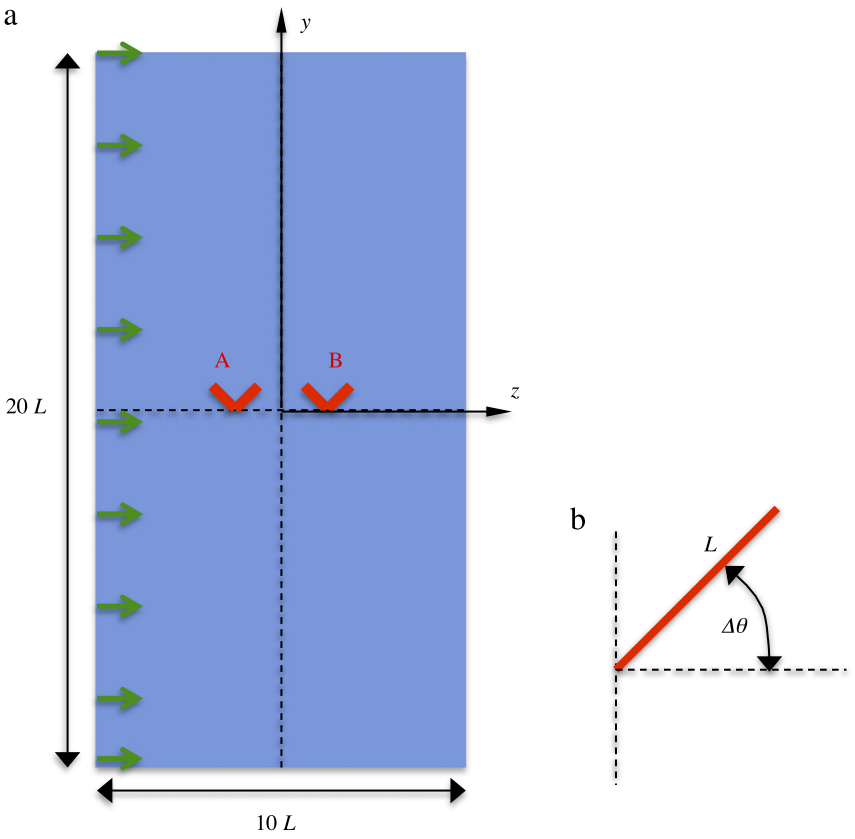

Fig. 1. Sketch of the problem definition. The green arrows denote the presence of a wind gust.

where $\mathbf{u}$ is the flow velocity and p is the fluid pressure. On the other hand, the center of mass of the wings can travel only in the vertical direction according to

$$M\ddot{y}(t) = F(t), \tag{4}$$

where y is the vertical component of the displacement of the center of mass of the wings and $F(t)$ is the time-dependent vertical component of the external forces which are exerted by the encompassing fluid on the solid body. Superimposed dots indicate the time derivatives.

2.2. The lattice Boltzmann-immersed boundary approach

The two-dimensional lattice Bhatnagar–Gross–Krook [13,32,33] equation is solved on a fixed square grid and the evolution of the particle distribution functions f_i, which are forced to move along prescribed directions i with velocities $\mathbf{c}_i$, is computed by

$$f_i(\boldsymbol{x} + \Delta t\mathbf{c}_i, t + \Delta t) = f_i(\boldsymbol{x}, t) + \frac{1}{\tau}\left[f_i^{eq}(\boldsymbol{x}, t) - f_i(\boldsymbol{x}, t)\right] + 3w_i\mathbf{c}_i \cdot \boldsymbol{g}(\boldsymbol{x}, t), \tag{5}$$

where $\boldsymbol{x}$ is the position and τ is the so-called relaxation parameter. The lattice direction vectors $\mathbf{c}_i$ are defined as

$$\mathbf{c}_i = 0, \quad \text{if } i = 0, \tag{6}$$

$$\mathbf{c}_i = [\cos((i-1)\pi/4), \sin((i-1)\pi/4)], \quad \text{if } i = 1, 3, 5, 7, \tag{7}$$

$$\mathbf{c}_i = \sqrt{2}[\cos((i-1)\pi/4), \sin((i-1)\pi/4)], \quad \text{if } i = 2, 4, 6, 8. \tag{8}$$

In this work, the so-called D2Q9 LB model is adopted, which forces the particle distribution functions to move along nine directions in two dimensions. The equilibrium particle distribution functions f_i^{eq} are derived in the form of a second-order expansion in the local Mach number [33], that is

$$f_i^{eq}(\boldsymbol{x}, t) = w_i\rho\left(1 + \frac{\boldsymbol{v} \cdot \mathbf{c}_i}{c_s^2} + \frac{(\boldsymbol{v} \cdot \mathbf{c}_i)^2}{2c_s^4} - \frac{\boldsymbol{v} \cdot \boldsymbol{v}}{2c_s^2}\right). \tag{9}$$

Once Eq. (5) is solved, the macroscopic fluid density ρ and the flow velocities $\boldsymbol{v}$ are computed as

$$\rho(\boldsymbol{x}, t) = \sum_i f_i(\boldsymbol{x}, t), \qquad \boldsymbol{v}(\boldsymbol{x}, t) = \frac{\sum_i f_i(\boldsymbol{x}, t)\mathbf{c}_i}{\rho(\boldsymbol{x}, t)}, \tag{10}$$

respectively. Notice that the relaxation parameter τ is strictly related to the fluid viscosity as $\nu = (\tau - 1/2)\, c_s^2$, being $c_s^2 = \sum w_i \mathbf{c}_i^2 = 1/3$ with w_i a set of 9 weights defined as $w_0 = 4/9$, $w_1 = w_2 = w_3 = w_4 = 1/9$ and $w_5 = w_6 = w_7 = w_8 = 1/36$. In order to account for the presence of the wings in the fluid lattice background, the immersed boundary method [14] is adopted. Let $\boldsymbol{X}_j$ denote the position of the jth individual. The IB method has been implemented in an implicit way in order to satisfy the no-slip condition. The iterative procedure [18,22] yields a correction term $\boldsymbol{g}(\boldsymbol{x}, t)$ to be used in the right-hand side of Eq. (5). Once $\boldsymbol{g}(\boldsymbol{x}, t)$ is computed, the force acting upon the body is immediately available as

$$\boldsymbol{F}_j = -\sum_{\boldsymbol{x}} \boldsymbol{g}(\boldsymbol{x}) W(\boldsymbol{x} - \boldsymbol{X}_j). \tag{11}$$

The adopted numerical methods are combined within a staggered explicit coupling algorithm. Its high properties in terms of continuity of tractions and velocities at the fluid–solid interface have been widely tested [22,24], showing that the proposed strategy is highly accurate and efficient.

3. Results and discussion

In this section, results from a numerical campaign are discussed. Each wing consists of 100 lattice nodes and it is represented by 200 Lagrangian immersed boundary points. Moreover, the grid consists of 1000 and 2000 lattice nodes in the horizontal and vertical directions, respectively. The value of the relaxation parameter is set to $\tau = 0.515$, thus corresponding to a Reynolds number $\mathcal{R}e = v_{tip}L/\nu = 200$, where $v_{tip} = 4L\Delta\theta/T$. All the LB simulations are carried out at low Mach number $\mathcal{M}a$, i.e. $\mathcal{M}a = v_{tip}/c_s = 0.0173$. Simulations stop when A or B overcomes the fluid domain limits. A and B are placed symmetrically with respect to the vertical direction. Each one is 100 lattice nodes far from the vertical axis of symmetry, y. In the wind gust is neglected, outflow boundary conditions are used at each edge of the fluid domain. Otherwise, at the westmost section a constant, uniform, and rightward velocity profile v_w is prescribed, which is enforced by the scheme proposed by Ref. [34]. The initial phase angle for the butterfly A is set to $\phi = 0^\circ$, while the one corresponding to B assumed different values, i.e. $\phi = 5^\circ, 10^\circ, 20^\circ, 30^\circ$.

First, the wind gust is neglected, i.e. $v_w = 0$. In Fig. 2 the time histories of the centers of mass of A and B are depicted for different values of the initial phase angle ϕ of B. For comparison, in each graph the scenario corresponding to an in-sync scenario, i.e. $\phi = 0^\circ$ for both A and B, is shown. As it is possible to observe, in the scenario characterized by $\phi = 10^\circ$ A experiences a fast take-off during the overall time history. On the other hand, B shows a similar behavior until $t/T \leq 8$; then, a slight disadvantage is experimented with respect to the in-sync scenario. In the remaining configurations, i.e. $\phi = 5^\circ, 20^\circ, 30^\circ$, both A and B benefit from the asynchronous motion, especially at $\phi = 20^\circ$, where the fast take-off is achieved. Notice that in each graph the time histories of A and B tend to intersect each other, i.e. A overtakes B or vice versa. Only at $\phi = 30^\circ$ this behavior is avoided, since B achieves higher positions rather than A during the whole time range.

Then, the wind gust is considered. In Figs. 3 and 4 the time histories of A and B in the off-sync scenarios are depicted by accounting for a lateral wind gust equal to $v_w = 0.001$ and $v_w = 0.002$, respectively. It is worthwhile to highlight that all the off-sync configurations correspond to faster take-off with respect to the in-sync conditions. Again, the scenario characterized by $\phi = 20^\circ$ is the most advantageous. In addition, notice that at $\phi = 10^\circ$ A and B show very close time histories of the position of the centers of mass if $v_w = 0.001$, whereas for $v_w = 0.002$ this behavior is addressed for the lowest value of ϕ, i.e. $\phi = 5^\circ$.

In Fig. 5, at $v_w = 0.005$ B gets higher positions than A during the overall time range at $\phi = 5^\circ, 20^\circ, 30^\circ$. Moreover, both A and B benefit from the off-sync motion. If $\phi = 10^\circ$ a drastically different graph is shown, which is characterized by a disadvantage experienced by the tandem of flapping wings, especially from A. If $v_w = 0.01$ is considered (see Fig. 6), remarkably different results are achieved. The scenario characterized by $\phi = 20^\circ$ confirms to be the most advantageous, since it is the only one providing a benefit with respect to the in-sync flight conditions. At $\phi = 5^\circ, 10^\circ$, slower take-offs are experimented, whereas at $\phi = 30^\circ$ the time histories of the off-sync condition are dramatically different, since A and B tend to translate downward. In Fig. 7 the behavior addressed in the previous figure is confirmed for $v_w = 0.02$. Specifically, at $\phi = 5^\circ, 10^\circ$, A and B show progressively arduous flight conditions, whereas at $\phi = 30^\circ$ the tandem goes downward, again. The remarkable differences are found at $\phi = 20^\circ$. In particular, such an off-sync scenario has proved to be the most advantageous in the above discussed configurations, whereas here it is shown that A and B both go downward. Thus, it is possible to assess that the wind gust dramatically affects the flight conditions, by playing a crucial deleterious role especially for high values of ϕ.

In Figs. 8 and 9, the velocity field is depicted for the whole spectrum of the investigated scenarios. It is worthwhile to notice that vortexes move progressively rightward as the wind gust increases. The more attractive feature that emerges from these pictures is that A and B appear to be supported by the vorticity during the travel. Notice that useful vortexes are strictly placed below the wings during the wingbeat. Therefore, the role of the tip-induced vorticity is confirmed to be crucial for the flight performance.

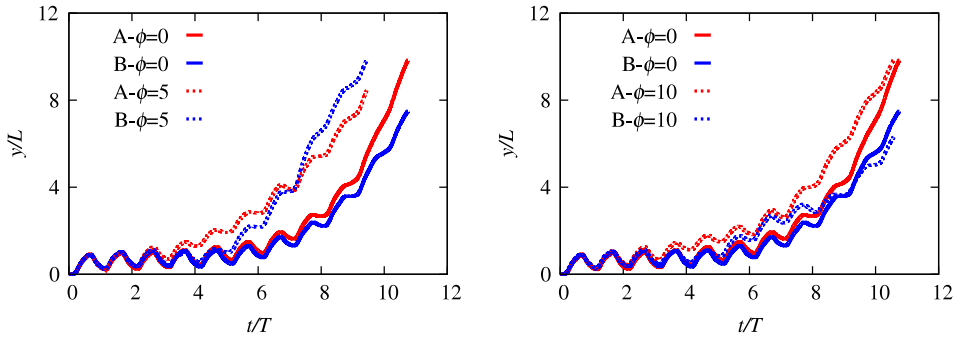

(a) $\phi = 5°$.

(b) $\phi = 10°$.

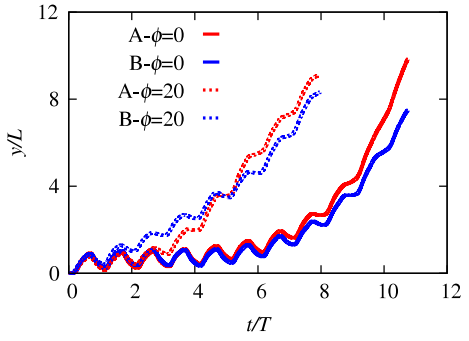

(c) $\phi = 20°$.

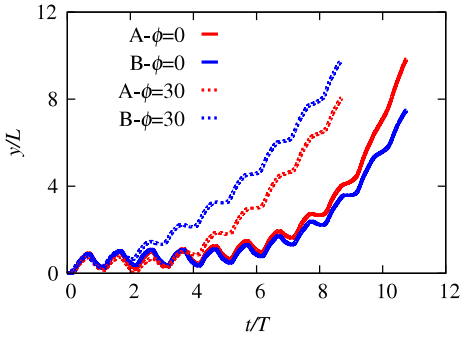

(d) $\phi = 30°$.

Fig. 2. Position of the centers of mass for different values of ϕ. $v_w = 0$.

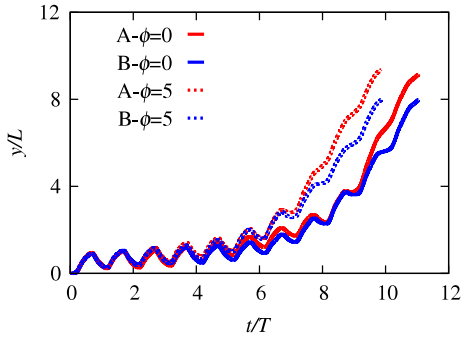

(a) $\phi = 5°$.

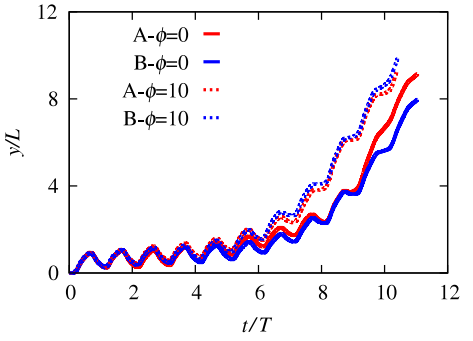

(b) $\phi = 10°$.

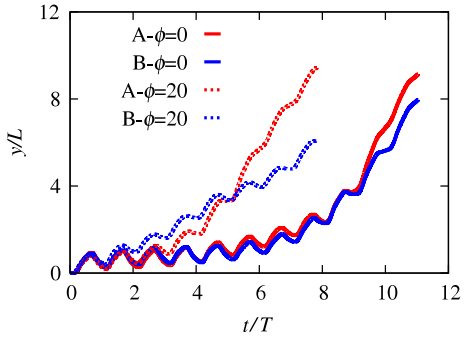

(c) $\phi = 20°$.

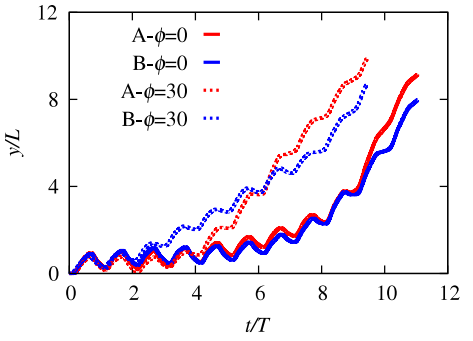

(d) $\phi = 30°$.

Fig. 3. Position of the centers of mass for different values of ϕ. $v_w = 0.001$.

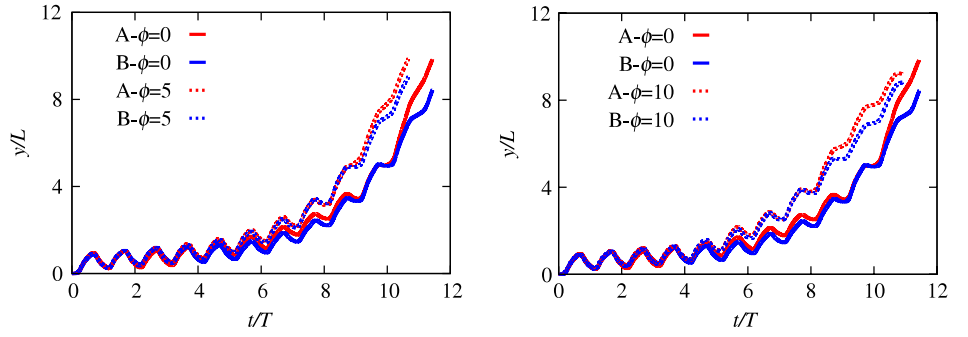

(a) $\phi = 5°$.

(b) $\phi = 10°$.

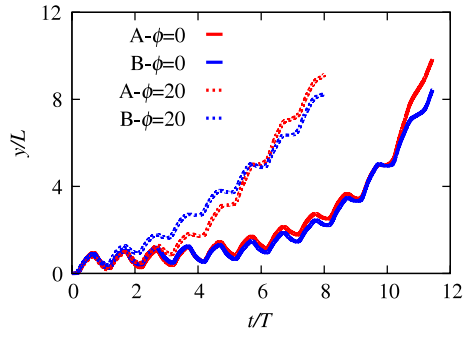

(c) $\phi = 20°$.

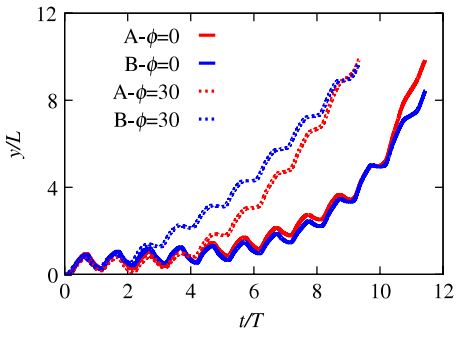

(d) $\phi = 30°$.

Fig. 4. Position of the centers of mass for different values of ϕ. $v_w = 0.002$.

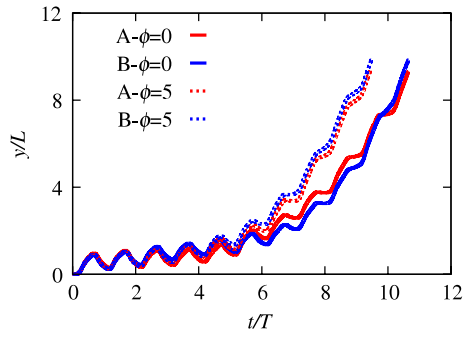

(a) $\phi = 5°$.

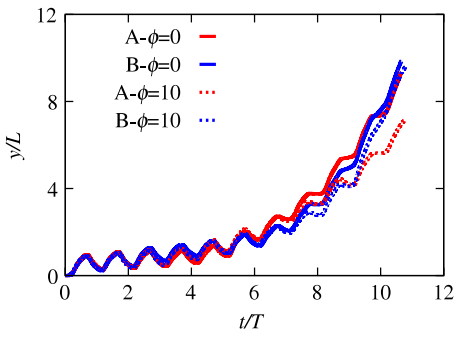

(b) $\phi = 10°$.

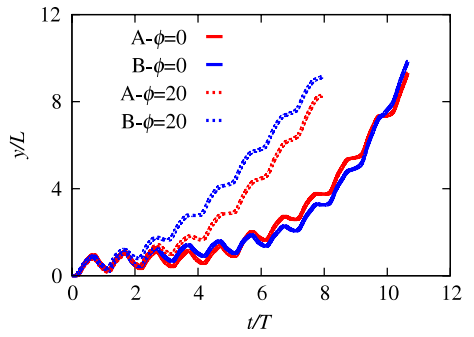

(c) $\phi = 20°$.

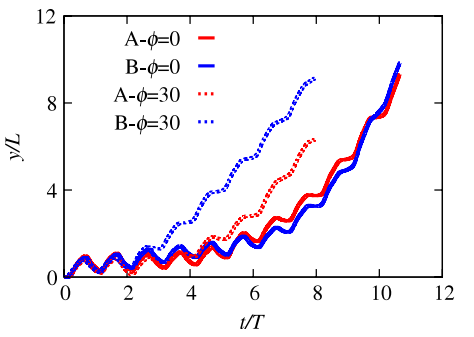

(d) $\phi = 30°$.

Fig. 5. Position of the centers of mass for different values of ϕ. $v_w = 0.005$.

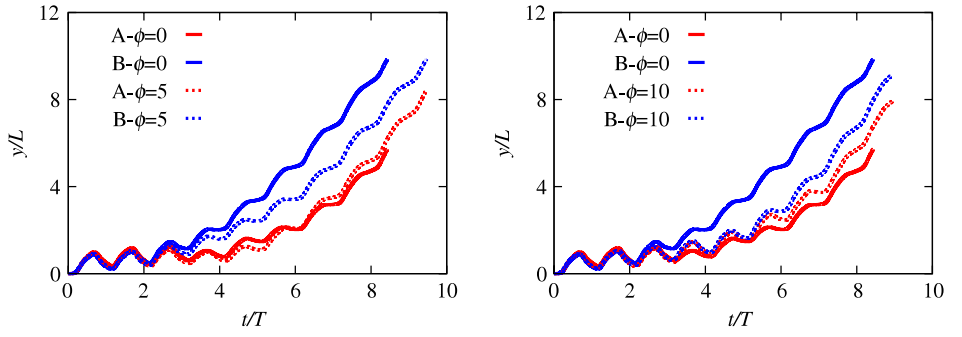

(a) $\phi = 5^\circ$.

(b) $\phi = 10^\circ$.

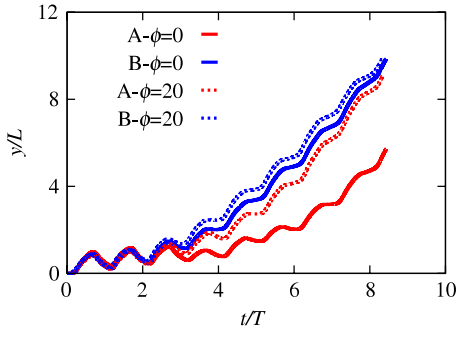

(c) $\phi = 20^\circ$.

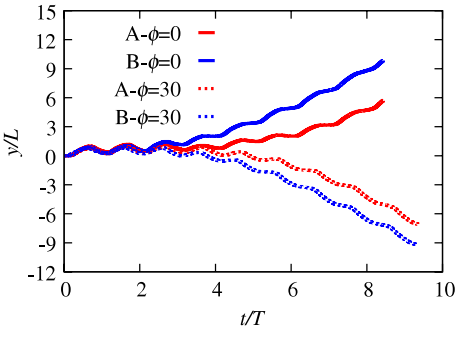

(d) $\phi = 30^\circ$.

Fig. 6. Position of the centers of mass for different values of ϕ. $v_w = 0.01$. At $\phi = 30^\circ$ a critical threshold $v_{tip}/v_w = 1$ is identified.

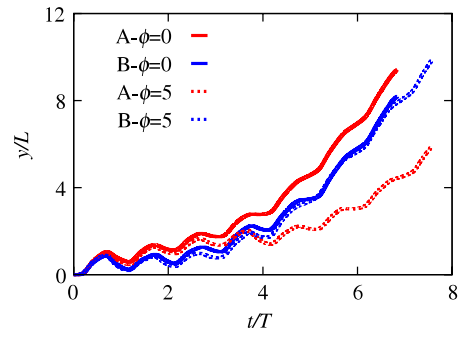

(a) $\phi = 5^\circ$.

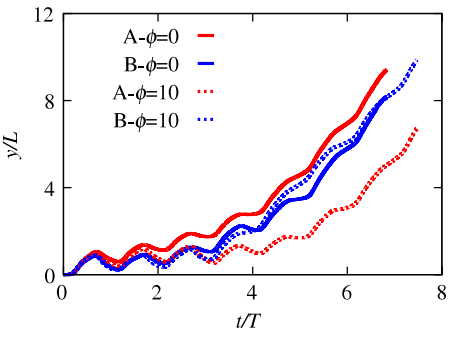

(b) $\phi = 10^\circ$.

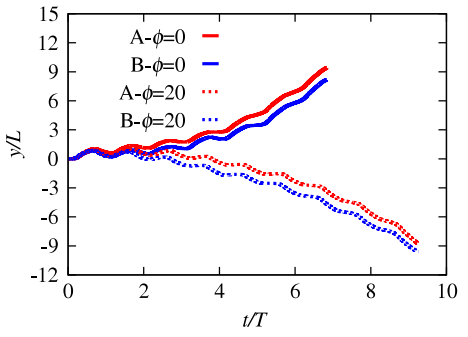

(c) $\phi = 20^\circ$.

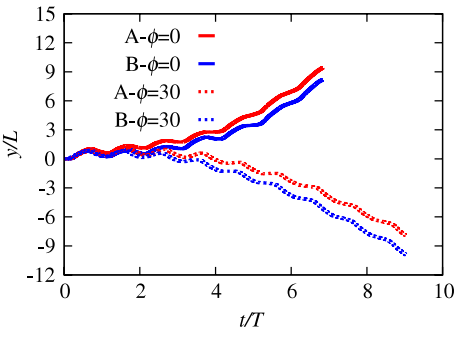

(d) $\phi = 30^\circ$.

Fig. 7. Position of the centers of mass for different values of ϕ. $v_w = 0.02$. At $\phi = 20^\circ$ a critical threshold $v_{tip}/v_w = 0.5$ is identified.

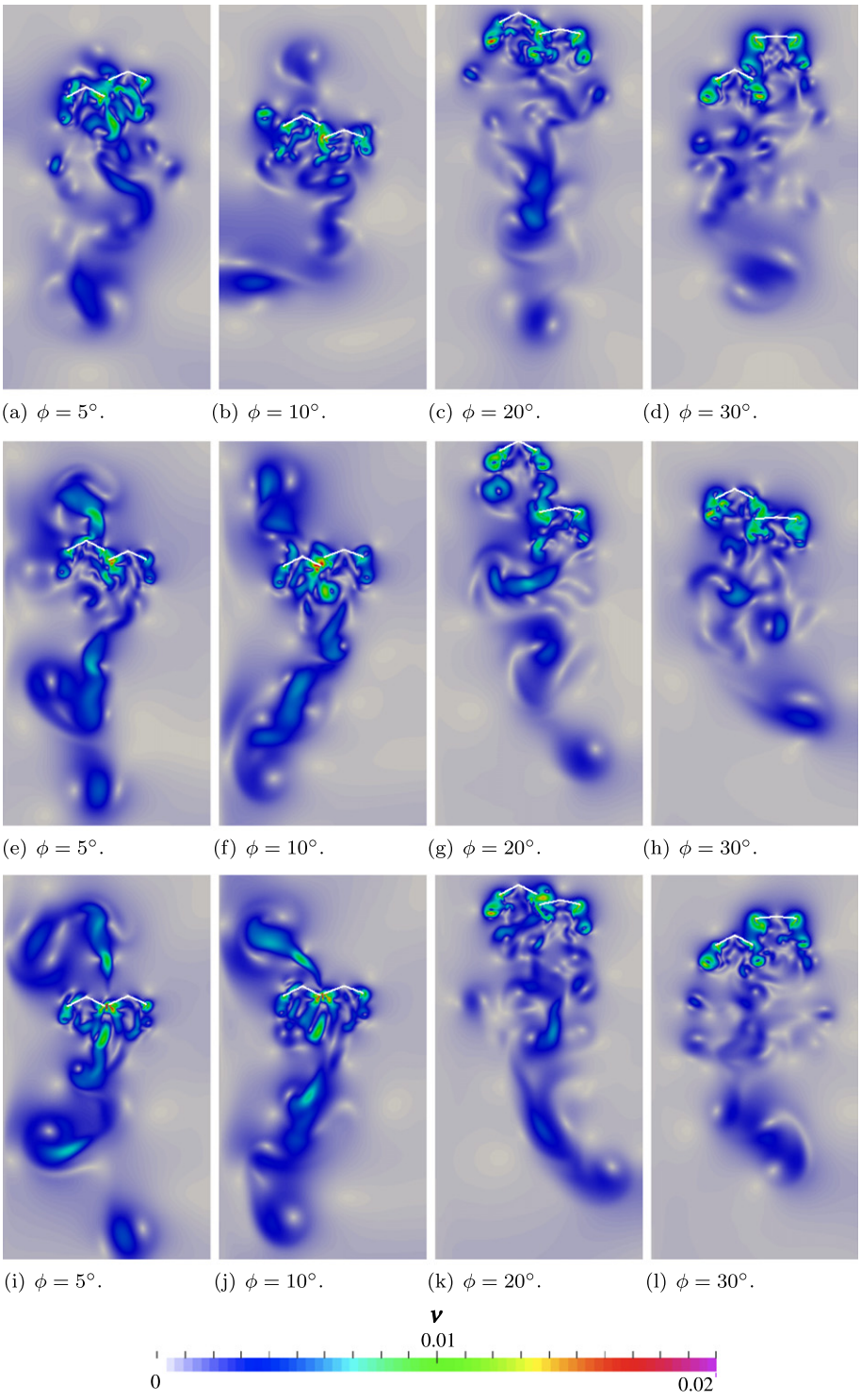

Fig. 8. Velocity field for different values of wind gust $t/T = 7.65$: $v_w = 0$ (first row), $v_w = 0.001$ (second row), $v_w = 0.002$ (third row).

For the sake of comparison, the scenario characterized by $v_w = 0.02$ is investigated by imposing $\phi = 20°$ and $\phi = 0°$ for A and B, respectively. In Fig. 10, the time history of the position of the centers of mass is depicted. As it is possible to observe, the deleterious effects of $v_w = 0.02$ vanish, since both A and B benefit from the wind gust. Therefore, it is possible to assess that the initial phase angle mutually affects both the bodies, giving an advantage. The corresponding velocity field is depicted in Fig. 11 at different time instants.

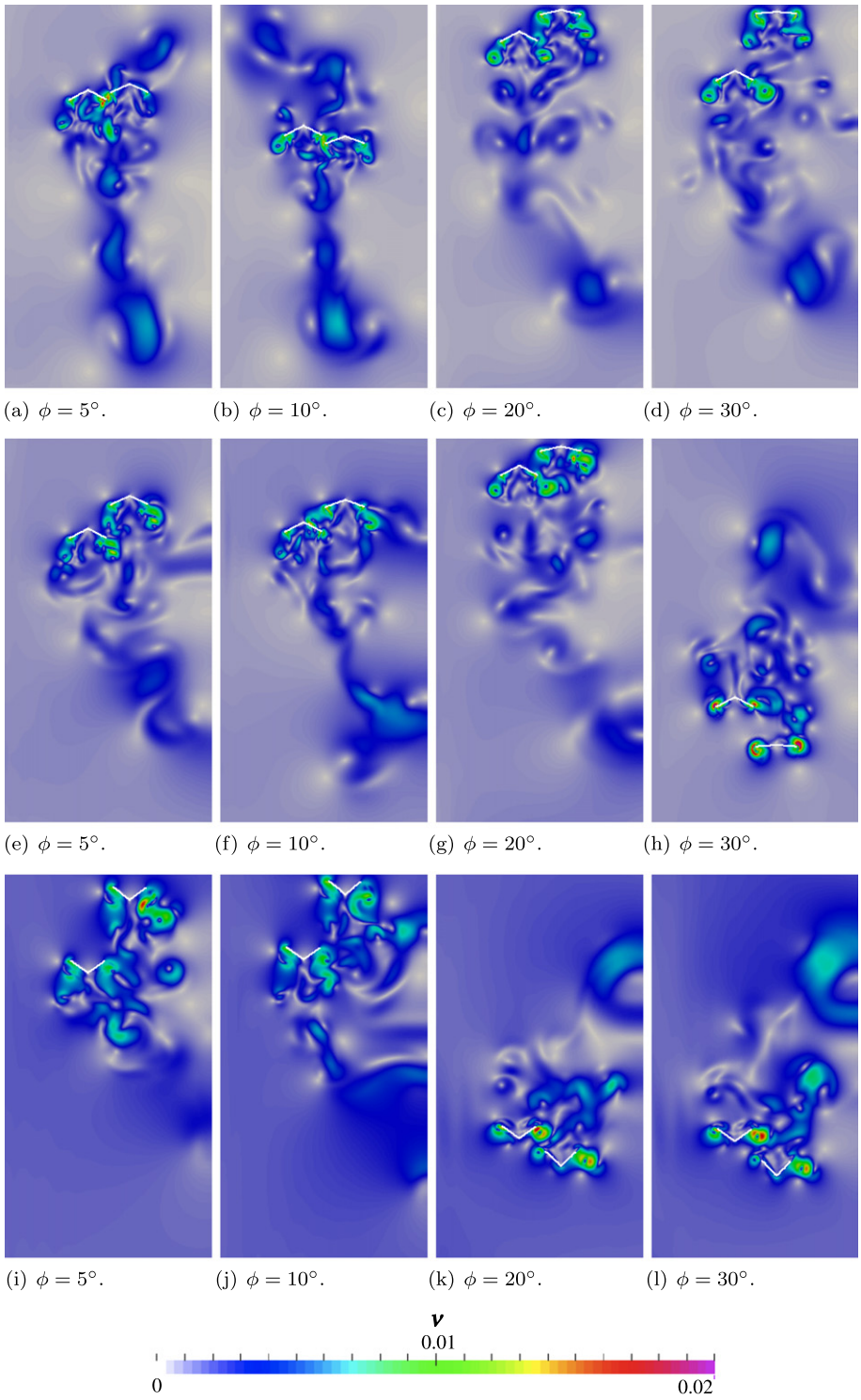

Fig. 9. Velocity field for different values of wind gust: $v_w = 0.005$, $t/T = 7.65$ (first row), $v_w = 0.01$, $t/T = 7.65$ (second row), $v_w = 0.02$, $t/T = 6.89$ (third row).

4. Conclusions

In this work, the flight performance of a tandem of asynchronous butterfly-like flapping wings has been investigated. According to previous efforts carried out by the author, the LB, IB and TDG methods have been properly combined to compute

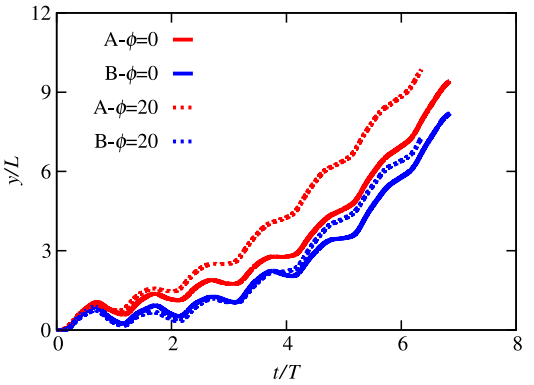

Fig. 10. Position of the centers of mass for $\phi = 20^\circ$ and $\phi = 0^\circ$ for A and B, respectively. $v_w = 0.02$.

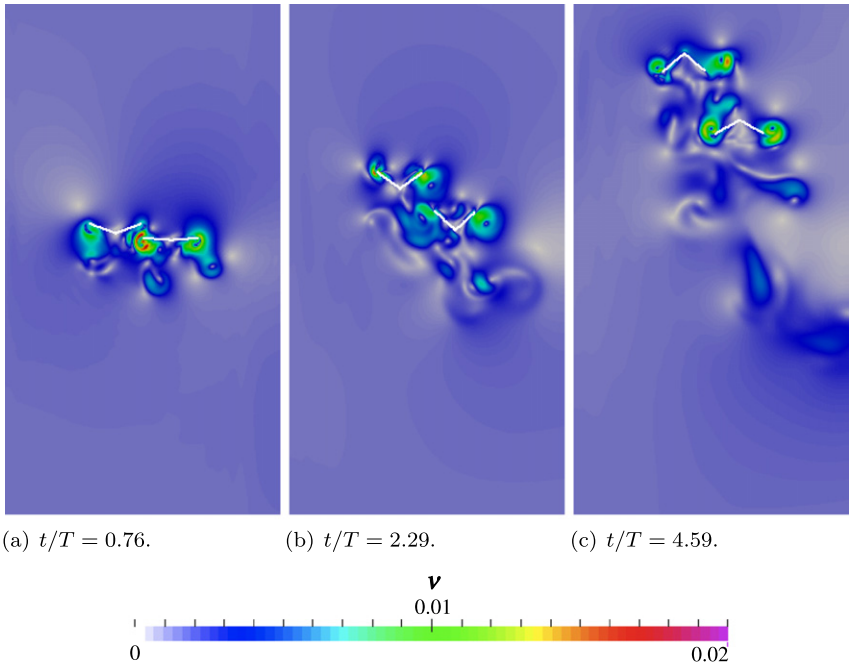

Fig. 11. Velocity field for $v_w = 0.02$ at $t/T = 0.76, 2.29, 4.59$. The values of the initial phase angle are $\phi = 20^\circ$ and $\phi = 0^\circ$ for A and B, respectively.

the vertical position of the centers of mass of the wings due to an imposed harmonic motion. Scenarios characterized by different values of the initial phase angle ϕ of the right wings (B) have been discussed by considering various values of a rightward wind gust v_w. It has been shown that the problem is strictly dependent on the ϕ and v_w. Specifically, increasing values of v_w tend to negatively affect the flight performance, independently of the value of ϕ, whereas for low values of the wind gust the tandem benefits from the asynchronous harmonic oscillations. Unlike previous efforts, the present work overcomes classical studies concerning isolated bodies, whereas it deeply investigates the mutual interaction of a tandem of symmetric flapping wings, elucidating the crucial role played by the initial phase angle difference.

Appendix. Validation of the LB–IB approach for flapping wing dynamics

According to Ref. [27], a single butterfly is considered. The hinge connecting the wings is placed in the center of the fluid domain. Fig. 12 shows the time history of the wing position for $\mathcal{R}e = 40$ and $\mathcal{R}e = 200$. In the case of $\mathcal{R}e = 40$ the grid consists of 1440×720 lattice nodes and the wings are discretized by using 60 elements (although rigid, the discretization is needed to evaluate the force distribution and to handle moving boundaries); in the case of $\mathcal{R}e = 200$ the dimensions are 1920×960 and 80 elements are used. For both simulations, the Mach number is $\mathcal{M}a = \frac{v_{tip}}{c_s} = 0.0162$. The relaxation parameter is set to $\tau = 0.542$ at $\mathcal{R}e = 40$ and to $\tau = 0.5112$ at $\mathcal{R}e = 200$. As can be observed in Fig. 12, very close agreement between the present solution and the results obtained in Ref. [27] is achieved. Notice that at $\mathcal{R}e = 200$ the wings successfully translate the flapping wing system away from its starting location, while at $\mathcal{R}e = 40$ they tend to oscillate about a fixed position.

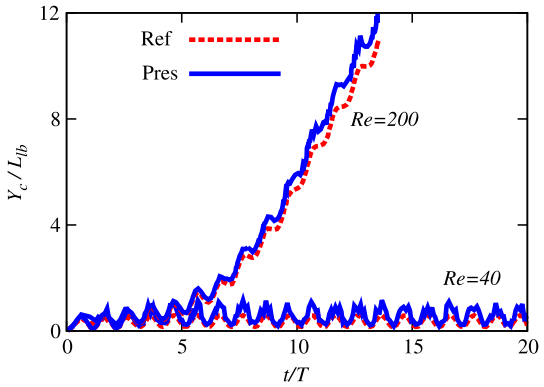

Fig. 12. Effect of the Reynolds number. Y_c/L_{lb} is the position of the center of mass normalized with respect to the length of the wing in lattice units L_{lb}. Ref and Pres account for reference and present values, respectively.

References

[1] S. Heathcote, I. Gursul, Flexible flapping airfoil propulsion at low Reynolds numbers, AIAA J. 45 (2007) 1066–1079.
[2] S. Heathcote, Z. Wang, I. Gursul, Effect of spanwise flexibility on flapping wing propulsion, J. Fluids Struct. 24 (2008) 183–199.
[3] L. Zhao, Q. Huang, X. Deng, S.P. Sane, Aerodynamic effects of flexibility in flapping wings, J. R. Soc. Interface 7 (2010) 485–497.
[4] A.M. Mountcastle, S.A. Combes, Wing flexibility enhances load-lifting capacity in bumblebees, Proc. R. Soc. B 280 (2013).
[5] C.-k. Kang, W. Shyy, Scaling law and enhancement of lift generation of an insect-size hovering flexible wing, J. R. Soc. Interface 10 (2013).
[6] A. Brodsky, Vortex formation in the tethered flight of the peacock butterfly inachis io l.(lepidoptera, nymphalidae) and some aspects of insect flight evolution, J. Exp. Biol. 161 (1991) 77–95.
[7] J.M. Birch, M.H. Dickinson, Spanwise flow and the attachment of the leading-edge vortex on insect wings, Nature 412 (2001) 729–733.
[8] R.J. Bomphrey, N.J. Lawson, N.J. Harding, G.K. Taylor, A.L. Thomas, The aerodynamics of manduca sexta: digital particle image velocimetry analysis of the leading-edge vortex, J. Exp. Biol. 208 (2005) 1079–1094.
[9] R.J. Bomphrey, N.J. Lawson, G.K. Taylor, A.L. Thomas, Application of digital particle image velocimetry to insect aerodynamics: measurement of the leading-edge vortex and near wake of a hawkmoth, Exp. Fluids 40 (2006) 546–554.
[10] F. Muijres, L. Johansson, R. Barfield, M. Wolf, G. Spedding, A. Hedenström, Leading-edge vortex improves lift in slow-flying bats, Science 319 (2008) 1250–1253.
[11] M. Fuchiwaki, T. Kuroki, K. Tanaka, T. Tababa, Dynamic behavior of the vortex ring formed on a butterfly wing, Exp. Fluids 54 (2013) 1–12.
[12] P. Trizila, C.-K. Kang, H. Aono, W. Shyy, M. Visbal, Low-reynolds-number aerodynamics of a flapping rigid flat plate, AIAA J. 49 (2011) 806–823.
[13] S. Succi, The Lattice Boltzmann Equation for Fluid Dynamics and Beyond, Clarendon, 2001.
[14] C. Peskin, The immersed boundary method, Acta Numer. 11 (2002) 479–517.
[15] A. De Rosis, Lattice Boltzmann simulations of flapping wings: the flock effect and the lateral wind effect, Int. J. Mod. Phys. C 8 (2014).
[16] O. Filippova, D. Hänel, Lattice Boltzmann simulation of gas-particle flow in filters, Comput. Fluids 26 (1997) 697–712.
[17] R. Mei, L. Luo, W. Shyy, An accurate curved boundary treatment in the lattice Boltzmann method, J. Comput. Phys. 155 (1999) 307–330.
[18] A. De Rosis, S. Ubertini, F. Ubertini, A comparison between the interpolated bounce-back scheme and the immersed boundary method to treat solid boundary conditions for laminar flows in the lattice boltzmann framework, J. Sci. Comput. (2014).
[19] A. De Rosis, G. Falcucci, S. Ubertini, F. Ubertini, S. Succi, Lattice Boltzmann analysis of fluid–structure interaction with moving boundaries, Commun. Comput. Phys. 13 (2012) 823–834.
[20] M. Mancuso, F. Ubertini, An efficient integration procedure for linear dynamics based on a time discontinuous Galerkin formulation, Comput. Mech. 32 (2003) 154–168.
[21] A. De Rosis, G. Falcucci, S. Ubertini, F. Ubertini, A coupled lattice boltzmann-finite element approach for two-dimensional fluid–structure interaction, Comput. Fluids 86 (2013) 558–568.
[22] A. De Rosis, F. Ubertini, S. Ubertini, A partitioned approach for two-dimensional fluid–structure interaction problems by a coupled lattice Boltzmann-finite element method with immersed boundary, J. Fluids Struct. 45 (2014).
[23] A. De Rosis, Analysis of blood flow in deformable vessels via a lattice Boltzmann approach, Int. J. Mod. Phys. C 25 (2013).
[24] A. De Rosis, A lattice boltzmann-finite element model for two-dimensional fluid–structure interaction problems involving shallow waters, Adv. Water Resour. 65 (2014).
[25] A. De Rosis, G. Falcucci, M. Porfiri, F. Ubertini, S. Ubertini, Hydroelastic analysis of hull slamming coupling lattice boltzmann and finite element methods, Comput. Struct. 138 (2014) 24–35.
[26] K. Srinivas Rao, M. Subrahmanya, D. Kulkarni, B. Rajani, Numerical simulation of turbulent flow past micro air vehicle wing sections (2009).
[27] K. Ota, K. Suzuki, T. Inamuro, Lift generation by a two-dimensional symmetric flapping wing: immersed boundary-lattice boltzmann simulations, Fluid Dyn. Res. 44 (2012) 045504.
[28] T. Inamuro, Y. Kimura, K. Suzuki, Flight simulations of a two-dimensional flapping wing by the ib-lbm, Bull. Am. Phys. Soc. 57 (2012).
[29] Y. Kimura, K. Suzuki, T. Inamuro, Flight simulations of a two-dimensional flapping wing by the ib-lbm, Int. J. Mod. Phys. C 25 (2014).
[30] S. Sunada, K. Kawachi, I. Watanabe, A. Azuma, Performance of a butterfly in take-off flight, J. Exp. Biol. 183 (1993) 249–277.
[31] T. Iima, M. Yanagita, Asymmetric motion of a two-dimensional symmetric flapping model, Fluid Dyn. Res. 36 (2005) 407–425.
[32] F.J. Higuera, S. Succi, R. Benzi, Lattice gas dynamics with enhanced collisions, Europhys. Lett. 9 (1989) 345–349.
[33] R. Benzi, S. Succi, M. Vergassola, The lattice Boltzmann equation: theory and applications, Phys. Rep. 222 (1992) 145–197.
[34] Q. Zou, X. He, On pressure and velocity boundary conditions for the lattice boltzmann bgk model, Phys. Fluids (1994-present) 9 (1997) 1591–1598.